Surface Characterization of PPTA Fibers Using Inverse Gas Chromatography

Miguel A. Montes-Morán,* Juan I. Paredes, Amelia Martínez-Alonso, and Juan M. D. Tascón

Instituto Nacional del Carbón, CSIC, Apartado 73, 33080 Oviedo, Spain

Received January 15, 2002

ABSTRACT: This work concerns the surface characterization of poly(*p*-phenylene terephthalamide) (PPTA) fibers, either with or without finish, and submitted or not to washing with acetone or to oxygen plasma treatment. These materials were studied by inverse gas chromatography (IGC) at infinite dilution using nonpolar (C_6−C_{12} *n*-alkanes) and polar molecules with different acid−base characteristics (tetrahydrofuran, toluene, carbon tetrachloride, acetone, *tert*-butyl alcohol). Complementary information was obtained by atomic force microscopy (AFM) and X-ray photoelectron spectroscopy (XPS). Results showed that the presence of a standard finish strongly decreases the surface energy of the PPTA fibers and confers them a more acidic character. Surfaces similar in structural and chemical properties to those of the pristine fibers can be obtained by solvent washing. Oxygen plasma treatment of PPTA produces strong changes in adsorption energetics (indicative of pore formation) and in surface nanomorphology, globular-like structures being formed. At the same time, an increase in the number of acidic and basic sites, identified as oxygenated functionalities (especially alcohol/ether groups), was detected. The capability of the used methodologies, particularly IGC, to follow changes in the surface properties of polymeric fibers is highlighted.

1. Introduction

High-performance aramids are among the strong, high-modulus, lightweight fibers that constitute a family of materials of widespread use in the commencing century. They are spun from lyotropic solutions of poly(*p*-phenyleneterephthalamide) or PPTA, containing highly oriented chains in their extended conformation due to intermolecular hydrogen bonds. This led to fibers showing a fibrillar hierarchy, with a high degree of crystallinity and crystal orientation, that confers exclusive material properties such as high strength, high modulus, and good chemical and flame resistance. Furthermore, comprehensible structure−property relationships have been found for this type of fibers.[1,2]

Apart from their use as such, aramid fibers are usually employed as reinforcing agents in organic matrix composites. It is well established that the characteristics of the fiber/matrix interface are a key factor for the performance of composites. For example, a good level of adhesion is required to transfer external loads effectively from the matrix to the fibers. Although composite design involves numerous factors, it seems necessary to characterize the thermodynamic and chemical states of the fiber surface, as well as to determine the effect of these surface properties on the final response of the material. Fiber producers understand the relevance of such a knowledge, devoting substantial research to characterize and modify material surface properties.[3]

Several methods have been investigated to improve the adhesion between aramid fibers and thermosetting or thermoplastic matrices. The development of specific coatings or finishes is possibly the most explored route. These finishes are designed to accomplish several purposes, from fiber protection and handling, to the enhancement of fiber activity in adhesion-related problems. The mentioned alternative entails the deposition of proprietary compounds on the surface of the aramid fibers at the final stages of fiber production (hence called finish). In fact, the process is fully implemented in fiber production lines, and it is relatively rare to obtain finish-free fibers commercially, i.e., fibers with no coating on their surfaces. Thus, different solvents are usually recommended to obtain "clean" aramid surfaces. The effect of such a solvent extraction on the final properties of the fiber is also an important subject of investigation.[4]

The use of cold plasma treatments constitutes a promising and attractive process to improve fiber activity. Plasmas contain highly reactive species and electromagnetic radiation which are able to interact with surfaces of polymeric materials. This highly reactive environment causes interatomic bonds to break, leaving radical species in the polymeric chains which are prone to initiate further reactions. As a consequence of these interactions, substantial surface modifications such as changes from hydrophobic to hydrophilic surfaces can be observed. Obviously, the degradation of fiber mechanical properties would be a potential drawback of this technique. However, plasma treatments carried out under controlled conditions of input radiation power, time of treatment, and type of gas employed limit their influence to the outermost layers of the fiber, thus minimizing negative influences on fiber bulk properties. Additionally, this type of treatments is clean, safe and environmentally friendly.[5]

The main objective of this work was to get some further insight into the effects of fiber finish and oxygen plasma treatment on aramid fibers. For this, adsorption of relevant probes on the fiber surfaces was studied by means of inverse gas chromatography (IGC). IGC constitutes an ideally suited technique to study adsorption at very low coverage (infinite dilution), and has demonstrated its usefulness for the surface characterization

* Corresponding author. E-mail: miguel@incar.csic.es. Telephone: + 44 985 11 90 90. Fax: + 44 985 29 76 62.

10.1021/ma020069m CCC: $22.00
Published on Web 05/22/2002

of a wide range of materials, especially polymers.[6−10] Other surface characterization techniques such as atomic force microscopy (AFM) and XPS were eventually employed to obtain as much complete information on the differences between the surfaces of the samples under study as possible.

2. Experimental Section

2.1. Materials. The PPTA fibers used in this study were in the form of Kevlar 29 1670 dtex (DuPont de Nemours Intl. S.A.), with typical values of 3.6 and 83 GPa for their tensile strength and modulus, respectively. The two starting samples were standard Kevlar 29 (subsequently referred to as sample K29 in this work), as well as its finish-free version (K29FF). The surface of this last sample K29FF can be thus considered to be pristine PPTA and as mentioned before is not commercially available. Manufacturer filament diameter values were approx 12 μm for both K29 and K29FF fibers.

Two additional aramid fiber samples, prepared from the starting materials K29 and K29FF, were also characterized. On one hand, yarns of K29 were thoroughly washed on-column with liquid acetone (approx 60 mL), at room temperature, to remove the finish from the fiber surface (sample K29W). On the other hand, 1000 filament yarns of the K29FF fibers were treated in a cold oxygen plasma environment. This plasma treatment was performed in a Technics Plasma 200-G cylindrical reactor, equipped with a microwave power generator working at a frequency of 2.45 GHz. Typical operational conditions were 75 W of microwave radiation power during 3 min of exposure, with 100 Pa pressure of O_2 (99.999% pure). Herein, fibers prepared following this plasma treatment will be referred to as sample K29O.

2.2. Methods. Adsorption measurements were carried out by IGC at infinite dilution using a Hewlett-Packard 5890-II gas chromatograph equipped with a high sensitivity (10^{-12} mol) flame ionization detector. Continuous fiber yarns (0.7−1 g) were packed into approximately 40 cm long passivated nickel columns (2.31 mm in internal diameter). Helium (99.9995% pure) was used as carrier gas. The gas flow rate F (15−20 mL min^{-1}) was measured at the column outlet (F_{flo}) by using a bubble flowmeter. Corrections were made for temperature difference between the column (T) and the flowmeter (T_{flo}), water vapor pressure of the bubble (P_w), and pressure drop (j correction factor, with P_{out} and P_{in} being the pressure at the outlet and inlet, respectively):[11]

$$F = jF_{flo}\frac{T}{T_{flo}}\left[\frac{(P_{out} - P_w)}{p_{out}}\right] \quad (1)$$

$$j = \frac{3}{2}\left[\frac{(P_{in} - P_{out})^2 - 1}{(P_{in} - P_{out})^3 - 1}\right] \quad (2)$$

Adsorption experiments were carried out at 10 K intervals in the 303−343 ± 0.05 K temperature interval. Small amounts (0.1−1 μL) of vapors of *n*-alkanes (C_6−C_{12}) (>99% pure) measured with a 10 μL Hamilton syringe were eluted through the columns. Changes in the surface chemistry were evaluated by injecting several polar probes of different acid−base characteristics (tetrahydrofuran, toluene, carbon tetrachloride, acetone, *tert*-butyl alcohol, purity >99%). At least five injections of each probe were carried out at each temperature. No variation was detected in the retention volume of the probes when different flow rates were used. This indicates that adsorption equilibrium was attained.[11] Prior to the IGC experiments, the chromatographic columns were conditioned by heating at 373 K under a constant helium flow (~20 mL min^{-1}). Typical conditioning times of 12 h were necessary to achieve reproducible results. The helium flow through the columns was not interrupted anytime in the course of the experiments in order to prevent further contamination of the fibers after column conditioning.

Atomic force microscopy (AFM) measurements were performed in the contact mode of operation in air at room temperature. Bundles of fibers were attached to sample holders by means of adhesive tape and then transferred to a Nanoscope Multimode IIIa (Digital Instruments), where AFM imaging was carried out. Special care was taken to avoid the presence of fibers bulging from the sample surface that could interfere with the cantilever and prevent the attaining of a stable AFM signal. The images were acquired in the constant force mode (variable height) to obtain topographical information on the surface. Microfabricated Si_3N_4 cantilevers (spring constant, $k = 0.06$ N m^{-1}) with integrated pyramidal tips were employed. To minimize the force imparted by the AFM tip against the sample surface and thus reduce sample disturbance to a minimum, force-vs-distance curves were regularly obtained to adjust the force. To corroborate the reproducibility of the images and check that the observed features were not a consequence of tip artifacts, all the samples were studied with several different previously unused tips and the images were collected in many different areas of every sample.

XPS surface characterization was carried out on a VG ESCALAB MK1 spectrometer using Al Kα radiation (energy 1486.6 eV) in a vacuum of 10^{-7} Torr and with the axis of the energy analyzer at 90° relative to the nominal plane of sample surfaces and operated in fixed transmission mode. An X-ray power of 200 W (10 mV and 20 mA) was used for all analyses. Correction was made due to angular asymmetry of the photoemissions, transmission of the energy analyzer, element photoionization cross section, and the inelastic mean free path of the photoelectrons.[12] Continuous yarns of the different fibers were rolled on aluminum stubs and clamped using a metallic clip. Surface atomic compositions were calculated from the areas of relevant peaks from survey scan spectra after fitting of a Shirley background. Spectra were averaged from three to five experiments with signals being accumulations of five scans each (step 0.3 eV and dwell time of 50 ms). All spectra have been energy calibrated by assigning 284.6 eV to the main C−H/C−C component of the C 1s line to eliminate charging effects. Nevertheless, the effect of sample charging was measured to be very similar to all fibers tested. High-resolution spectra for C 1s, O 1s, and N 1s lines were signal averaged accumulations of 200 scans with a pass energy of 25 eV, a 0.05 eV step, and a dwell time of 50 ms. The envelopes were curve fitted using mixed Lorentzian−Gaussian curves, after fitting of a Shirley background, using Grams/32 (Galactic Inc.) data processing software.

3. Results

3.1. Adsorption of *n*-Alkanes at Zero Coverage. Unlike conventional adsorption techniques, IGC allows the measurement of adsorption data down to very low vapor concentrations, where the surface coverage approaches zero and adsorbate−adsorbate interactions are negligible. The chromatographic peaks obtained for the *n*-alkanes were mainly symmetrical for all samples under study, with no dependence of the peak maximum position on the amount of probe molecule injected. Under these conditions the adsorption can be considered to take place in the linear part of the isotherm (Henry's law), and the retention time of the different *n*-alkanes could be measured at the peak maximum.[11] The Henry's law constant, K_s, that characterizes the adsorption equilibrium, is related directly to the retention volume by

$$V_N = K_s A \quad (3)$$

where A is the total surface area of the stationary phase. The previous equation is valid as long as the bulk absorption of the probe in the stationary phase is negligible.[11] Thermodynamic functions of the adsorption process at infinite dilution can be thus calculated from

K_s. The standard free energy of adsorption, ΔG^0_a was computed according to the following expression

$$\Delta G_a^{\ 0} = -RT \ln(K_s p_{s,g}/\pi_s) \quad (4)$$

where $p_{s,g}$ (pressure of the gas phase) and π_s (spreading pressure of the adsorbed gas) are constant parameters determined by the reference state. In this work, values proposed by de Boer[13] were used ($p_{s,g} = 101$ kN m^{-2}; $\pi_s = 0.338$ mN m^{-1}). The Brunauer−Emmett−Teller BET (N_2, 77 K) specific surface area of all Kevlar fibers were measured to be 0.23 m^2 g^{-1}. This value coincides with the specific geometric area of the fibers, assuming a fiber diameter of 12.2 μm. It must be stressed here that no change in BET surface area could be detected after the plasma treatment of the fibers.

When zero coverage (or infinite dilution) conditions are fulfilled the standard differential heat of adsorption, q^0_d is numerically equal to the opposite of the enthalpy of the process. This value can be obtained from the variation of ΔG^0_a with temperature. For an equilibrium process this variation is given by the Gibbs−Helmholtz equation,

$$\left[\frac{\partial(-\Delta G_a^{\ 0}/T)}{\partial(1/T)}\right]_p = \left[R\,\frac{\partial(\ln K_s)}{\partial(1/T)}\right]_p = q_d^{\ 0} \quad (5)$$

Figure 1 illustrates the linear dependence of ln K_s as a function of (1/T) obtained for the adsorption of *n*-nonane on the aramid fiber samples under study. This behavior, extensive to the rest of studied hydrocarbons, implies that q^0_d is constant within the temperature range. The standard deviations in q^0_d values obtained in this way were never larger than 1%.

Values of standard free energies of adsorption of *n*-alkanes at 323 K are given in Table 1. The tendency observed for all the fibers was consistent over the whole temperature interval studied (303−343 K), although only data at 323 K are shown for simplicity. Also included in Table 1 are the values of the differential heats of adsorption at zero coverage of the different linear alkanes on the Kevlar samples.

From the adsorption standard free energies and standard enthalpies, adsorption entropies were calculated straightforwardly according to

$$\Delta S_a^{\ 0} = -\frac{(q_d^{\ 0} + \Delta G_a^{\ 0})}{T} \quad (6)$$

Table 2 gives ΔS^0_a values obtained in this way. In agreement with the linearity in ln K_s vs (1/T) plots (Figure 1), the adsorption entropies were independent of temperature. Values given in Table 2 are the average of data calculated at the different temperatures, deviations being smaller than 1%.

Values of the dispersive component of the surface free energy, γ^D_S were calculated using the formula proposed by Gray[14]

$$\frac{-\Delta G^{CH_2}{}_a}{N_A a(CH_2)} = 2\,(\gamma(CH_2)\gamma_S^{\ D})^{1/2} \quad (7)$$

where $\Delta G^{CH_2}{}_a$ is the difference in the free energy of adsorption of two *n*-alkanes with succeeding values of n, N_A is Avogadro's number, $a(CH_2)$ is the area of one methylene group (0.06 nm^2), and $\gamma(CH_2)$ is the surface tension of ideal liquid polyethylene. Figure 2 illustrates the linear variations of $-\Delta G^0_a$ (at 323 K) with the number of carbon atoms in the series of *n*-alkanes used as probes. The slope of the regression lines corresponds to $-\Delta G^{CH2}{}_a$ for the different fibers, at a given temperature. Calculated γ^D_S values are plotted in Figure 3 for the various PPTA fibers within the range of temperature studied. As mentioned previously in the case of other thermodynamic magnitudes, the error in γ^D_S values is very small (1−2%) due to the excellent data correlations obtained, similar to those shown in Figure 2.

From the results shown in Figure 3, the dependence of γ^D_S with temperature could be established. In all cases, it was found that linear expressions fit the experimental data reasonably well. Results corresponding to the linear regression of the data obtained for the different aramid samples are collected in Table 3. Values of γ^D_S at 293 K were subsequently calculated by extrapolation, and they are also included in Table 3.

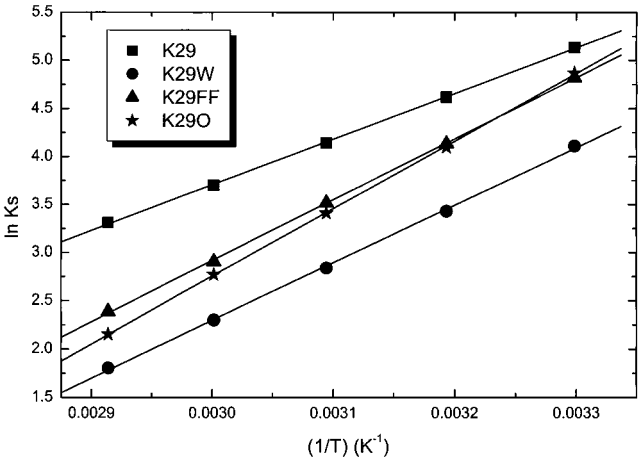

Figure 1. Variation of lnK_s with (1/T) for the adsorption of *n*-nonane on aramid fiber samples.

Table 1. Standard Free Energies and Differential Heats of Adsorption of *n*-Alkanes on the Different Fibers (Free Energy at 323 K)

fiber	*n*-alkane	$-\Delta G^0_a$ (kJ mol^{-1})	q^0_d (kJ mol^{-1})	$-\Delta H_{Liq}$ (kJ mol^{-1})[a]
K29	C_7	21.5	30.3	36.7
	C_8	24.0	35.0	41.5
	C_9	27.0	39.6	46.4
	C_{10}	29.0	44.2	51.4
	C_{11}	31.0	47.5	56.4
	C_{12}			61.5
K29W	C_7			
	C_8	20.1	45.9	
	C_9	23.0	49.8	
	C_{10}	25.8	55.8	
	C_{11}	28.7	61.7	
	C_{12}	31.7	65.5	
K29FF	C_7	18.6	39.5	
	C_8	21.7	47.5	
	C_9	24.8	52.8	
	C_{10}	27.9	59.2	
	C_{11}	31.0	63.9	
	C_{12}			
K29O	C_7	18.3	50.1	
	C_8	21.4	56.6	
	C_9	24.5	58.5	
	C_{10}	27.5	65.4	
	C_{11}	30.6	68.4	
	C_{12}			

[a] Heats of liquefaction.

Table 2. Standard Entropies of Adsorption of *n*-Alkanes on the Different Samples

fiber	*n*-alkane	$-\Delta S^0_a$ (J K^{-1} mol^{-1})	$-\Delta S^0_a$ (J K^{-1} mol^{-1})[a]
K29	C_7	27.3	52.4
	C_8	33.8	53.0
	C_9	40.5	53.5
	C_{10}	47.2	53.9
	C_{11}	49.9	54.3
	C_{12}		54.7
K29W	C_7		
	C_8	80.0	
	C_9	82.7	
	C_{10}	92.5	
	C_{11}	101.9	
	C_{12}	104.7	
K29FF	C_7	64.5	
	C_8	80.2	
	C_9	86.6	
	C_{10}	97.0	
	C_{11}	101.8	
	C_{12}		
K29O	C_7	98.3	
	C_8	108.7	
	C_9	105.1	
	C_{10}	116.9	
	C_{11}	117.1	
	C_{12}	124.8	

[a] Standard entropy of adsorption (at 303 K) calculated according to de Boer's model (eqs 4 and 5).

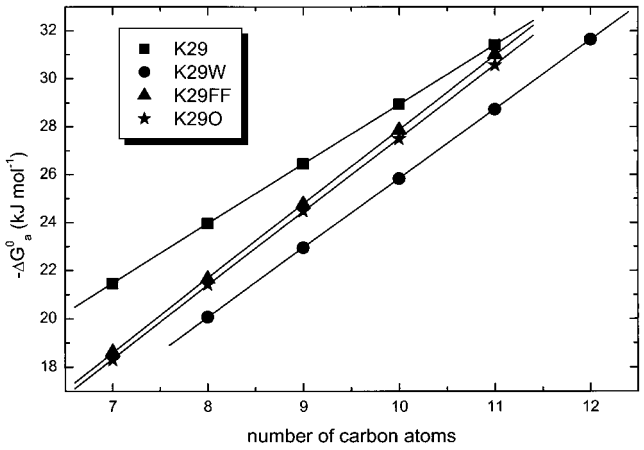

Figure 2. Variations of the standard adsorption free energy ($-\Delta G^0_a$) with the number of carbon atoms in *n*-alkanes ($-\Delta G^0_a$ data at 323 K).

3.2. Adsorption of Polar Probes at Zero Coverage. Whereas adsorption of *n*-alkanes takes place through dispersive interactions thus rendering information related to fiber microstructure (i.e., fiber degree of crystallinity), polar probes are needed to determine the acid−base character of the fiber surfaces. The adsorption of these molecules on the stationary phase is influenced, not only by dispersive interactions, but also by additional specific contributions. These specific contributions include dipole−dipole and acid−base interactions (or electron acceptor−donor effects), the latter ones involving much higher energies than the former ones.[15] In fact, it is usually assumed that the specific contribution of the adsorption of polar probes are actually acid−base interactions only. The ability of these polar molecules to donate or accept electrons has been parametrized by means of the so-called donor number (DN) and acceptor number (AN), respectively.[15] Table 4 contains the DN and AN parameters of the probes

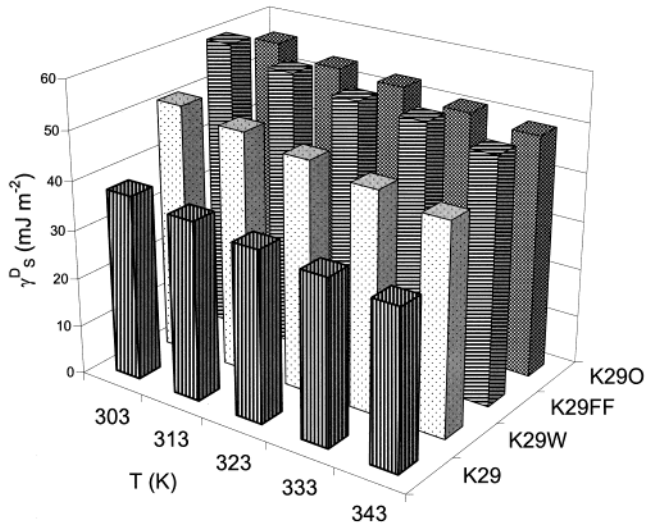

Figure 3. Dispersive component of the surface free energy of aramid fibers at various temperatures.

Table 3. Dependence of γ^D_S (mJ m^{-2}) with Temperature (K) for All the PPTA Fibers under Study

fiber		*r*	γ^D_S (mJ m^{-2})[a]
K29	$\gamma^D_S = 81.1-0.142\ T$	0.999	39.5
K29W	$\gamma^D_S = 116.4-0.214\ T$	1.000	53.7
K29FF	$\gamma^D_S = 128.3-0.227\ T$	0.990	61.8
K29O	$\gamma^D_S = 107.0-0.168\ T$	0.992	57.8

[a] Values extrapolated at $T = 293.15$ K.

Table 4. Donor Numbers (DN) and Acceptor Numbers (AN) of the Polar Probes Used in This Work

probe	AN (kJ mol^{-1})	DN (kJ mol^{-1})
THF	2.1	83.7
toluene	0.7	0.4
CCl_4	2.9	0
acetone	10.46	71.1
t-butyl alcohol	31.8	

used in this work, as well as their acid−base character (according to these numbers).[15,16]

Slight concentration-dependent effects were observed for the elution of polar probes through all chromatographic columns, except in the case of the standard K29 fiber. As a result, elution peaks of some of the compounds tested were asymmetric. The origin of this asymmetry should be the so-called "slow kinetic processes",[11] rather than being associated with instrumental problems (dead volumes in the detector or injector, imperfect column packing, etc.). Slow kinetic processes are characteristic of markedly energetically heterogeneous surfaces containing preferential sites where desorption takes place in a slower fashion. They correspond to nonequilibrium situations so that the gas flow rate will have a significant effect on them. Different flow rates were tested, but no totally satisfactory results were obtained. Moreover, it was observed that the degree of asymmetry decreased dramatically when working at extremely low probe concentrations, i.e., at low signal-to-noise ratio levels. Retention times were therefore estimated from the first momentum of peaks obtained at such conditions.

Similar thermodynamic properties to those described for the elution of linear alkanes can be obtained for the polar probes injected. Figure 4 shows the variation of $\ln K_s$ vs $(1/T)$ for all the polar probes on the K29 sample.

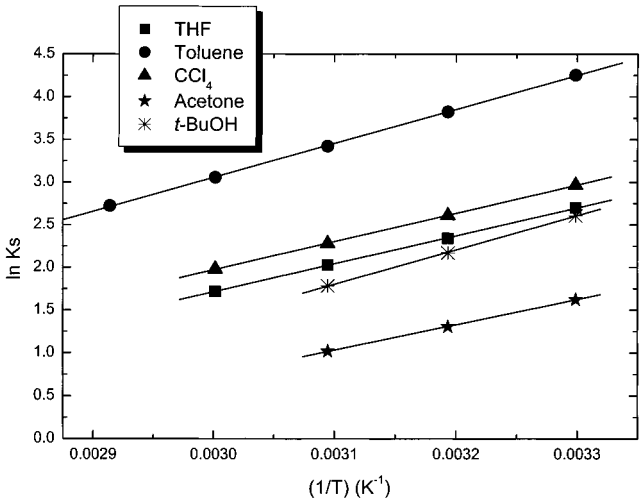

Figure 4. Variation of $\ln K_s$ with $(1/T)$ for the adsorption of different polar probes on K29 (standard Kevlar 29) sample.

Table 5. Differential Heats of Adsorption q°_d (kJ mol^{-1}) of Several Polar Probes on Aramid Surfaces

	K29	K29W	K29FF	K29O	$-\Delta H_{Liq}$ (kJ mol^{-1})[a]
THF	27.5	44.0	53.9	56.1	32.2
toluene	33.1	37.6	50.9	46.6	38.0
CCl_4	27.6	33.6			32.4
acetone	24.5	44.6	55.1	55.5	31.3
tert-butyl alcohol	33.5	59.0	64.5	69.8	46.1

[a] Heats of liquefaction.

Similar plots were obtained for the rest of the fibers under study. As it can be noticed, reasonably good data regressions could be drawn. Values of standard enthalpies of adsorption (or differential heats of adsorption, eq 5) were then calculated from the slopes of the lines depicted in Figure 4. Table 5 shows the heats of adsorption of the polar probes onto the Kevlar samples. Standard errors are once more relatively small, within the range of 2−3% of values collected in Table 5.

Two main components can be considered to contribute to the standard enthalpy of adsorption of polar probes, namely the specific contribution $\Delta H^{SP}{}_a$ and the dispersive contribution $\Delta H^{D}{}_a$:[17]

$$\Delta H^{0}{}_a = \Delta H^{SP}{}_a + \Delta H^{D}{}_a \qquad (8)$$

Several procedures have been developed in order to evaluate $\Delta H^{SP}{}_a$ from IGC measurements at zero surface coverage. Among them, the method proposed by Donnet et al.[18] seems to be more robust than the rest to account for the specific (acid−base) interaction of polar probes adsorbed on relatively high energetic surfaces. This method takes into account the molecular polarizability of the different polar adsorbates. Specific interactions $(-\Delta G^{SP}{}_a)$ are first determined, at a given temperature, from differences between $-\Delta G^{0}{}_a$ values of the polar probes and the reference line composed with data obtained from the elution of *n*-alkanes. An example of such a calculation is depicted in Figure 5, where the alkane line corresponds to the series from C_6 to C_{10}. Pertinent $-\Delta G^{SP}{}_a$ data for all fibers, at 303 K, are plotted in Figure 6.

$-\Delta H^{SP}{}_a$ can be now computed from the variation of $(-\Delta G^{SP}{}_a/T)$ vs $(1/T)$, as stated in eq 5. This type of plot, corresponding to adsorption data of polar probes on the plasma oxidized aramid surface K29O, is shown in Figure 7. The slope of the lines also depicted in Figure 7 corresponds to the value of $-\Delta H^{SP}{}_a$ for a particular probe onto the aramid surface. Results obtained for the different systems under study are collected in Table 6. For the rest of the samples studied, regressions of data similar to those appearing in Figure 7 were rather poor, especially for the finish-free version of Kevlar 29

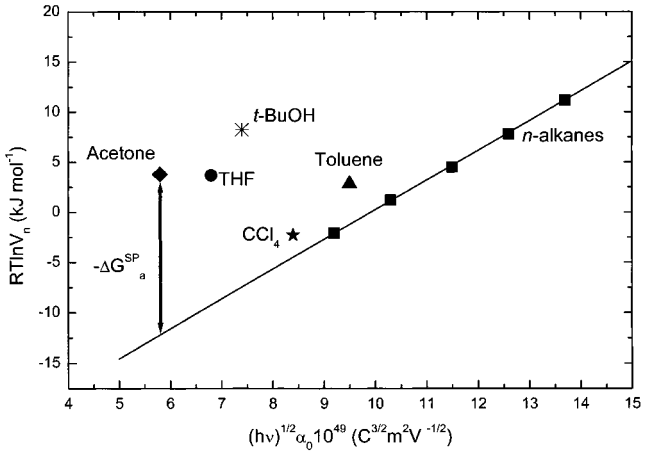

Figure 5. Graphical description of the method followed to obtain the specific contribution of the adsorption free energy $-\Delta G^{SP}{}_a$ measured for the different polar probes. The solid line corresponds to the *n*-alkane trend line.

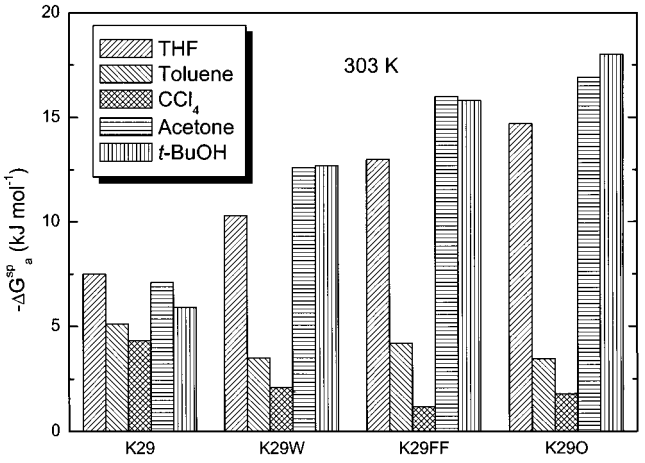

Figure 6. $-\Delta G^{SP}{}_a$ values calculated for the adsorption of different polar probes on the aramid surfaces under study, at 303 K.

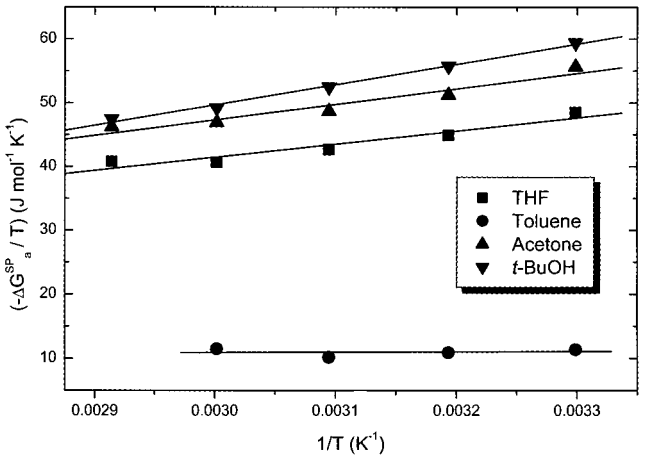

Figure 7. Variation of $(-\Delta G^{SP}{}_a/T)$ with $(1/T)$ for the adsorption of different polar probes on K29O (plasma-treated) sample.

Table 6. Specific (Acid−Base) Contribution to the Standard Enthalpy of Adsorption $-\Delta H^{SP}_a$ (kJ mol^{-1}) of Several Polar Probes on Aramid Surfaces

	K29	K29W	K29FF	K29O
THF	12.9 (0.9)	17.3 (2.0)	29.8 (6.8)	20.6 (3.5)
toluene	7.1 (0.5)	3.5 (1.8)	4.0 (4.2)	0.5 (3.3)
CCl_4	6.0 (0.8)	0.5 (2.5)		
acetone	15.4 (1.7)	22.4 (2.0)	36.0 (8.3)	24.3 (3.8)
tert-butyl alcohol	17.2 (1.0)	34.6 (4.2)	36.5 (5.6)	31.8 (1.5)

(sample K29FF). Individual standard errors are therefore included (in parentheses) in Table 6.

Herein values of $-\Delta G^{SP}_a$ and $-\Delta H^{SP}_a$ will be used as parameters to compare the acid−base character of the different aramid surfaces under study. These parameters can only account for qualitative changes in the surface chemistry of a given fiber. Further empirical approaches suggested by other authors would lead eventually to absolute parameters, similar to the AN and DN numbers mentioned before, describing in a quantitative manner the electron donor−acceptor properties of the solid surfaces. In the present work, this procedure has been discarded on operational basis. From the point of view of calculation, the errors associated with $-\Delta H^{SP}_a$ values restrict, in some cases, their use in further parameter estimations. In other cases, when $-\Delta H^{SP}_a$ errors are tolerable, we experienced similar problems to those described quite recently when calculating absolute parameters to account for the acid−base character of a solid surface: plots of $(-\Delta H^{SP}_a/AN)$ vs (DN/AN) of all polar probes tested lead to misleading results due to the substantial uncertainties of the final absolute parameters obtained.[4]

4. Discussion

4.1. Effect of Fiber Finish on the Surface Properties. Samples K29, K29W, and K29FF will be compared in this section in order to establish the effects of the finish on the surface characteristics of the PPTA fibers. Regarding the adsorption of linear alkanes, there exist qualitative differences in the thermodynamic parameters obtained for the K29 and the rest of fibers under consideration. Values of q^0_d (Table 1) are systematically the lowest ones for all the alkanes tested. Also shown in this table are the heats of liquefaction (ΔH_{Liq}) of the *n*-alkanes used, at 323 K. It can be observed that the differential heats of adsorption of the *n*-alkanes on K29W and K29FF fiber surfaces are larger than the heats of liquefaction, whereas lower values are obtained for the K29 fiber. The first behavior (i.e., $q^0_d > -\Delta H_{Liq}$) is typical of adsorption processes where adsorbate−adsorbent interactions are stronger than adsorbate−adsorbate interactions.[14] Assuming a multilayer model of adsorption, q^0_d results of K29W and K29FF (Table 1) confirm that adsorption takes place at a very low surface coverage. It is also expected that values of q^0_d approaching $-\Delta H_{Liq}$ will be obtained as the number of adsorbate layers on the fiber surface increases.

On the other hand, the behavior of the K29 fiber, with $q^0_d < -\Delta H_{Liq}$, might be considered anomalous; however, it has been reported several times before. Chappell and Williams, for example, found the same observation in all the aramid fibers with surface finishes characterized by them,[19] independently of the particular finish composition. They also concluded that the complete isotherm of adsorption of *n*-alkanes on this type of fibers (K29 in the present work) would be Type III type according to the Brunauer−Demming−Demming−Teller BDDT classification.[20] This type of adsorption is representative of weak dispersive adsorbate−adsorbent interactions.

A very similar conclusion can be reached from the analysis of the standard entropies of adsorption (Table 2). Also included in Table 2 are the adsorption entropy values predicted by an ideal adsorption model where the adsorbate is assumed to behave ideally as a bidimensional gas.[20] According to this, the variation in the standard entropy of adsorption will coincide with the entropy decrease predicted by the loss of one translational degree of freedom, i.e., the difference between the translational entropies of a tridimensional ($_3S_t$) and a bidimensional gas ($_2S_t$), as given, respectively, by the statistical thermodynamic eqs 9 and 10:

$$ {}_3S_t = R \ln(M^{3/2}T^{5/2}) - 9.62 \quad (9) $$

$$ {}_2S_t = R \ln(MTA_s) + 275.32 \quad (10) $$

where M is the molecular weight and A_s is the area occupied by one molecule in the standard adsorption state ($4.08T \times 10^{-16}$ cm^2). As Table 2 shows, the experimental adsorption entropies are larger (in absolute value) than those predicted by the theoretical estimation for the K29W and K29FF samples. This means that the adsorbed hydrocarbons are more ordered than as predicted by a bidimensional gas model, involving the additional loss of some vibrational and/or rotational degrees of freedom. In other words, adsorbed molecules have a mobility lower than that representing free movement over the surface, with consequent additional loss of some degree of freedom. On the contrary, K29 sample entropies of adsorption are lower than the theoretical prediction (Table 2). In this case, alkane molecules on the fiber surface are more disordered than the bidimensional gas model. That positive contribution to the entropy has been assigned to mixing between the adsorbed molecules and surface contaminants. It must be stressed here that the possibility of probe absorption (i.e., diffusion into the bulk material) is negligible due to the operational conditions of IGC at zero coverage.[11] This fact is confirmed by the elution behavior of the different alkanes tested on the K29 fiber (C_6−C_{12}). Peaks of each alkane, at different temperatures, were mainly symmetric, with maxima being independent of the quantity injected. Also a constant increment of the retention times with the length of the carbon chains was observed.

Results of q^0_d obtained for the K29FF sample are systematically higher than those corresponding to the acetone-washed sample (K29W), although differences are small (2−4 kJ mol^{-1}) (Table 1). This would indicate that the washing process is not effective in removing completely the finish material from the K29 fiber. Alternatively, it might be also considered that the solvent (acetone) has some effect on the microstructure of the outer layers of the aramid fiber. This possibility was suggested by Rebouillat et al.,[21] who found enthalpies of adsorption of *n*-alkanes onto finish-free versions of Kevlar 29 and Kevlar 49 fibers to be very close to the enthalpy of liquefaction (Table 1), especially for medium-length chain probes (*n*-heptane to *n*-decane). These results are, however, surprising in the light of the values obtained in the present work (Table 1) since, as mentioned above, such a behavior (i.e., $q^0_d \approx -\Delta H_{Liq}$) would be characteristic of weak adsorbate−adsorbent interactions. Moreover, q^0_d values reported by Chappell and

Table 7. Literature Values of γ^D_S Determined by IGC on Different PPTA Surfaces

sample	T (K)	γ^D_S (mJ m^{-2})	ref
Kevlar 49 (standard)	293	32.0, 37.5	22
Kevlar 49 (Soxhlet/acetone)		65.1	
Kevlar 29 (standard)	293	34.1−37.4	19
Kevlar 29 (Soxhlet/acetone)		57.7	
Kevlar 29 (standard)	323	34	23
Kevlar 29 (finish-free)		40	
Twaron[a] (sized fibers)	313	36.3,40.0	4
Twaron[a] (finish-free)		52.9	
Twaron[a] (Soxhlet/ethanol)		48.8	

[a] Akzo Nobel, Arnhem, The Netherlands.

Williams[19] on Kevlar 29 fibers Soxhlet extracted in acetone match, within experimental error, our results corresponding to the K29FF sample (Table 1). It seems then that the possibility of surface microstructure damage after acetone washing can be ruled out. On the other hand, it should confirm that the Soxhlet extraction is more successful for cleaning standard Kevlar 29 fibers than the procedure followed in the present work.

Analysis of the dispersive component of the PPTA fibers surface tension γ^D_S (which, for comparative purposes, can be considered as the difference between the free energies of alkanes differing in one methylene group) renders similar conclusions. This quantity is however slightly more sensitive to surface changes than the heats of adsorption (Table 1). From results of Figure 3, it appears now in a clearer manner that sample K29W is still quite different from sample K29FF. At this point, we thought interesting to compare our data with those found by other authors. Table 7 summarizes the γ^D_S results obtained also by IGC on different aramid fibers, already reported in the literature. When making such a comparison, various aspects must be kept in mind. Apart from differences arising from batch to batch, IGC is very responsive to the column pretreatment intended for cleaning fiber surfaces from physisorbed species, as mentioned in the Experimental section. All the results compiled in Table 7 were obtained after similar column pretreatments to that carried out in the present work, in terms of treatment time and temperature. Furthermore, the *absolute* value of γ^D_S calculated by means of eq 7 depends on the choice of both $a(CH_2)$ and $\gamma(CH_2)$ parameters, which are not unique. Although, the same area of the methylene group (0.06 nm^2) was used to calculate all values of Table 7, some authors [23] selected a different route to estimate $\gamma(CH_2)$, i.e., by extrapolating surface tension data of *n*-alkanes to infinite chain length (37.5 mJ m^{-2} at 293 K). This procedure underestimates the absolute value of γ^D_S by approximately 3 mJ m^{-2} with respect to the method followed in the present work (see Results).

Taking the previous considerations into account, several common outlines can be established after comparing our results (Figure 3 and Table 3) with the values collected in Table 4. First, it can be observed that all sized fibers exhibit γ^D_S values in the range 35−40 mJ m^{-2}, regardless of their origin (Kevlar and Twaron) or degree of crystallinity (Kevlar 29 and 49). As pointed out by Chappell and Williams after an extensive characterization of fibers coated by different surface finishes,[19] this is possibly due to the fact that the hydrophobic portion of the finish is the available adsorbent in these fibers. Since this hydrophobic portion would be constituted in the majority of cases by aliphatic chains, the apparent lack of sensitivity of these measurements to the exact nature of the surface finish should not be surprising. This also agrees with the low enthalpy of adsorption measured in the case of fiber K29 (Table 1). On the other hand, γ^D_S values of cleaned or finish-free fibers seems to depend mainly on fiber crystallinity. Thus, low modulus aramids (i.e., Kevlar 29) γ^D_S data at 293 K are within 57−61 mJ m^{-2}, whereas γ^D_S of higher modulus fibers (Kevlar 49) are well over 60 mJ m^{-2}. This is understandable on the basis that a higher level of surface crystallinity (and thus a higher modulus) enhances the interactions between the adsorbent and the linear alkanes. Assuming this, it can be predicted that Twaron fibers characterized in ref 4 are low modulus ones. From the data in Table 7, the high level of reproducibility of the surface characterization technique employed (IGC) should also be pointed out. Results of the finish-free version studied in the present work (fiber K29FF) coincide, within experimental error, with values obtained by Rebouillat et al on Kevlar 29 finish-free surfaces,[23] as well as those of the Kevlar 29 fiber Soxhlet extracted in acetone reported by Chappell and Williams.[19]

Contact angle measurements is the technique traditionally employed to estimate the surface tension γ_S of solids. When compared to the values obtained for aramid fibers from these measurements ($\gamma_S \approx 44$ mJ m^{-2} at 293 K),[24] values of the dispersive component of the surface free energy obtained in this work (Figure 3) are significantly higher, except for the K29 sample. Hence, the meaning of γ^D_S calculated by IGC at zero surface coverage can be questioned. The discrepancy can be explained, however, considering that the treatment of the columns, prior to the IGC experiments, leads to fiber surfaces free from adsorbed species and other possible contaminants. If these contaminants were present, as in the case of the wetting measurements, the value of γ^D_S should be notoriously reduced.[25] Besides that, the contribution of high energy sites will be significantly overweighed in IGC measurements under infinite dilution conditions. In fact, contact angle measurements are known to provide an average of the surface energy. It can be thus stated that the finish present in sample K29 contributes to homogenize the fiber surface from an energetic point of view, given that the γ^D_S value of K29 sample is similar to that expected from wetting measurements.

Apart from changes in the adsorption of the *n*-alkanes, sizings or finishes present on the fiber should also affect the polarity of its surface. Results of Table 5 reveal, for all polar probes tested, clear differences between the adsorption enthalpies of sample K29 and the rest of fibers studied. As in the case of the linear hydrocarbons, $q^0_d < -\Delta H_{Liq}$ for all polar probes eluted through the standard Kevlar 29 column, whereas the contrary is observed for the rest of aramid fibers. The same arguments thus prevail; i.e., weak adsorbate−adsorbent interactions are characteristic of the adsorption process of polar molecules onto K29 surfaces.

Direct comparison of differential heats of adsorption values of Table 5 can be misleading both between different polar probes within a given sample, or between the same probe and different aramid surfaces. The reason following the first is obvious since the molecular dimensions and polar character of the adsorbates are different. As for the second situation, a correct comparison could be only made if the magnitude of dispersive

Table 8. Atomic Percentages of Primary Elements (excluding H) of Several Aramid Samples

fiber	% C	% N	% O	% Na
K29	82.2	2.1	15.2	0.5
K29FF	83.8	7.0	9.2	
K29O	77.9	7.6	14.5	

interactions exerted by the solid surfaces is similar, which is not the case for the samples under study. These drawbacks are circumvented when specific components of thermodynamic quantities $-\Delta G^{SP}_a$ and $-\Delta H^{SP}_a$ are compared (Figure 6 and Table 6, respectively). As mentioned before, errors in $-\Delta G^{SP}_a$ data are much lower than those of $-\Delta H^{SP}_a$. Since trends followed by both magnitudes are broadly the same, it is preferable to discuss changes in polarity of the aramid fibers by the use of $-\Delta G^{SP}_a$ values (Figure 6). In doing so, several features appear to be relevant. Differences between $-\Delta G^{SP}_a$ data of sample K29 are relatively small, with all polar probes rendering values in the range 5−7 kJ mol^{-1}. When compared with the values obtained for the finish-free sample K29FF, an overall increase of $-\Delta G^{SP}_a$ is observed for all polar probes excluding toluene and CCl_4. This indicates that the surface finish present on fiber K29 reduces the number and/or strength of the surface acidic and basic sites of the bare K29FF fiber. Furthermore, sample K29W shows an intermediate behavior as it was also observed when the adsorption of linear alkanes was studied.

The use of specific parameters such as $-\Delta G^{SP}_a$ or $-\Delta H^{SP}_a$ does not allow one to establish the overall acidic or basic character of the fibers under study, as it was mentioned in the previous section (Results). However, qualitative changes in the acid−base character of different fibers can be ascertained by means of $-\Delta G^{SP}_a$ data. For example, it can be seen from Figure 6 that the basic character of the fiber increases after washing the finish off its surface. Indeed, the $-\Delta G^{SP}_a$ ratio of the basic (THF) to the acidic probe (*t*-BuOH) gives a clear indication of K29 surface being more acidic than K29W one. This trend is confirmed when fiber K29FF is taken into account. Hence, although the absolute value of $-\Delta G^{SP}_a$ for both THF and *t*-BuOH probes rises with respect to K29W, the ratio ΔG^{SP}_a(THF)/ΔG^{SP}_a(*t*-BuOH) is very similar to that of sample K29W. On the other hand, K29 fiber shows the highest specific contribution to the free energy of adsorption of the apolar molecules toluene and carbon tetrachloride when compared to the rest of samples, which in turn exhibit very similar values of $-\Delta G^{SP}_a$(Toluene) and $-\Delta G^{SP}_a(CCl_4)$. Such relatively high values of $-\Delta G^{SP}_a$(Toluene) and $-\Delta G^{SP}_a(CCl_4)$ obtained for the K29 fiber might be explained in terms of entropy contributions to the free energy of adsorption, since the $\pi-\pi$ and multipole interactions expected in the adsorption of toluene and carbon tetrachloride, respectively, would not amount to too much over pure dispersive interactions.

Since $-\Delta G^{SP}_a$ values measured by IGC provide only qualitative information on the variations in surface chemistry, the use of XPS as a complementary surface characterization technique could offer, in principle, a more detailed description. Table 8 collects the atomic percentages as measured by XPS analysis performed on three of the four aramid samples under study. Regarding fibers K29 and K29FF, differences in atomic concentrations are evident. The most relevant feature is the very low amount of atomic N on K29 surface, thus indicating that the surface exposed to the adsorption of the different probes in IGC experiments is very different from that of a pristine PPTA fiber. Also the high concentration of O suggest the occurrence of oxygenated functionalities in the finish material. IR analysis of extraction residues has shown aliphatic esters as a major component.[19] Finding of slight amounts of Na (Table 8) could be due to residual fiber processing products or presence of salts on the fiber finish.[19]

4.2. Effect of Plasma Treatment on the Surface Properties. Fibers K29FF and K29O are the relevant samples to be compared in order to evaluate the changes brought about by the plasma treatment. Following the same scheme depicted in the previous section, data of *n*-alkanes elution will be first discussed.

As it can be seen in Table 1, almost identical $-\Delta G^0_a$ were obtained for the adsorption of the linear alkanes on both K29FF and K29O fibers. This obviously results in surfaces with very similar values of γ^D_S (see Figure 3), calculated according to eq 5. There are however substantial differences regarding the adsorption of *n*-alkanes on both fibers, as confirmed by the other two thermodynamic magnitudes under consideration. Data collected in Table 1 reveal that sample K29O exhibits the highest values of differential heats of adsorption for all the hydrocarbons tested. Likewise, this fiber shows the highest standard entropies of adsorption when compared to the rest of samples (Table 2).

Surface treatments in general (and plasma oxidation in particular) bring about changes in both fiber microstructure and/or chemistry. Following well-established ideas of separate interfacial interactions in the field of surface chemistry and adhesion,[17] adsorption of *n*-alkanes on treated aramid fibers will give (in principle) information related to changes in fiber surface microstructure, due to the nonpolar character of these probes. The differential heat of adsorption of *n*-alkanes is related directly to the adsorption potential exerted by the microscopic structures, i.e., those to which the molecules have access. There exist well-established models accounting for the microstructure of aramid fibers. Regarding their surface, it is found that amorphous regions coexist along with well ordered crystallike regions.[1,2] The adsorption of *n*-alkanes onto each of these particular microstructures can be expected to be different; therefore, variations on their relative amount should be detected by means of IGC experiments. In other words, differences between q^0_d of K29FF and K29O surfaces (Table 1) might be explained in terms of different degrees of fiber surface crystallinity. Furthermore, IGC studies on Kevlar 49 fibers reported higher q^0_d values than those obtained for the low modulus (hence lower crystallinity) K29FF sample characterized in the present work (Table 1), with differences amounting to approximately 6 kJ mol^{-1}.[22,26] This would suggest that the plasma treatment did enhance the crystallinity of the bare K29FF fiber. This possibility can be reasonably discarded on the basis of the following arguments. A possible route to obtain a higher surface concentration of the crystallike regions vs the amorphous ones would involve selectivity of the plasma treatment. Although it can be assumed that the amorphous areas are much more reactive in general than the crystalline regions, the actual conditions of a plasma treatment are far too vigorous to lead to a considerable discrimination between them. For example, it is known that the atomic species present in an oxygen plasma are able to break strong C−C covalent bonds in pristine graphite.[27]

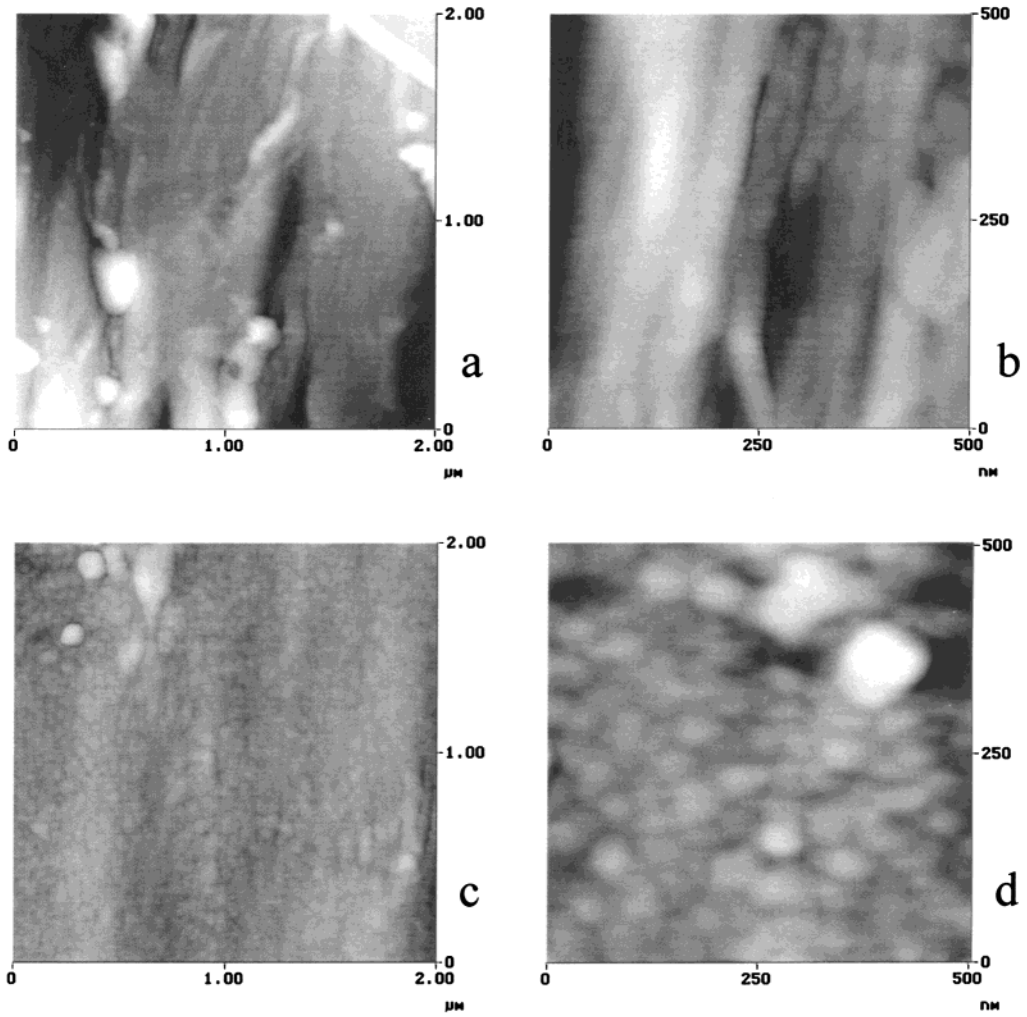

Figure 8. AFM micrographs (2000 × 2000 and 500 × 500 nm^2 areas) of (a, b) untreated K29FF sample and (c, d) plasma-treated K29O sample.

Another possible explanation to the hypothesis of enhancement of fiber crystallinity after the treatment would suggest a "cleaning off" mechanism; i.e., the plasma would remove the outer layers of the fiber and expose new areas of higher crystallinity. Recent X-ray microdiffraction studies have confirmed the existence of such a skin/core structure in Kevlar 29 fibers.[28] However, the degree of crystallite orientation decreases from skin toward the center of the filaments.[28] This is again in contradiction with the effect of the plasma treatment as described in the present IGC study.

A more plausible explanation for the increase of q^0_d values of K29FF after plasma treatment can be found taking into account the effect of the surface nanoroughness of the material on the adsorption of linear alkanes. To get some further insight into the morphological changes brought about by plasma treatment on the K29FF aramid fiber surface, an attempt was made to characterize the samples by the use of AFM. The nanometer scale topography of K29FF and K29O fibers could be resolved with this technique and significant differences were detected. Figure 8 shows four micrographs (2000 × 2000 and 500 × 500 nm^2 areas) corresponding to the K29FF and K29O samples. Both fiber surfaces exhibit clear dissimilarities even at the lower level of magnification (Figure 8, parts a and c). Surfaces of K29FF samples consist of relatively smooth areas coexisting with flaws and some contamination stains. The smooth areas present a fibrillar nanostructure which is characteristic of PPTA fibers.[29−31] Fibrils of approximately 30 nm in diameter running more or less parallel to the fiber axis are better observed at a higher magnification (Figure 8b). As mentioned in the Introduction, they are formed by the association of several PPTA chains through hydrogen-type intermolecular bonds.

Plasma-treated fiber K29O, on the other hand, exhibits a higher level of surface roughness (Figure 8c), with speckled areas substituting the smooth surfaces present on the untreated fibers (Figure 8a). The treatment has also removed the spots appearing in K29FF and assigned to surface contaminants. In addition, images obtained at 500 × 500 nm^2 (Figure 8d) reveal dramatic changes on fiber surface brought about by the plasma treatment. The fibrillar microstructures clearly observed in Figure 8b have disappeared in Figure 8d and are replaced instead by a globular-like morphology. These globular nanostructures have been also detected on other polymeric materials submitted to similar treatments.[32,33] It is thought that both high energy atomic species and radiation generated in the plasma environment cause polymeric bonds to break, leading to open short-chains prone to suffer further reactions. The round shape of the nanostructures of Figure 8d has been interpreted by Nie et al. as a result of the surface tension of liquidlike materials formed during the modi-

fication process.[32] Furthermore, work completed in our group has demonstrated that this globular type of structures is also characteristic of long time plasma treatments carried out on carbon materials such as carbon fibers.[34,35]

As mentioned before, occurrence of these micro and nanostructures must be related to the adsorption behavior of the *n*-alkanes onto the fiber surfaces. The higher degree of surface roughness of the plasma-treated fibers (K29O) with respect to the fresh ones (K29FF) might be responsible for the increase of the heats of adsorption for the linear alkanes. Indeed, the effect of the surface morphology on the final values of γ^{D}_{S} has been reported before by means of the elution of branched alkanes onto different solids.[36] The increase of surface roughness after the plasma treatment, as evidenced by Figure 8, parts c and d, encompasses the formation of high energy sites which can be considered as pores. It is known that the curvature of pore walls in microporous materials modifies the surface energy in comparison with that of a flat surface, resulting in a stronger adsorbent−adsorbate interaction.[37,38] What it is quite surprising in the case of the PPTA fibers characterized in this work is that the final values of γ^{D}_{S} for both untreated K29FF and treated K29O samples are essentially the same (Figure 3), however their heats (and entropies) of adsorption are rather different (Tables 1 and 2).

Nevertheless, it must be stressed that the micropore volume created after the plasma treatment could not be detected by using standard CO_2 adsorption isotherms (273 K) measured volumetrically (Quantachrome NOVA 1200 analyzer). The amount of micropores brought about by the plasma treatment would only affect the adsorption of the alkanes at a very low adsorbate concentration (close to zero surface coverage). A more detailed analysis of q^{0}_{d} and $-\Delta S^{0}_{a}$ values of Tables 1 and 2 provide further evidences of the existence of porous structures on the K29O surface. Differences between the heats of adsorption obtained for a given alkane on K29FF and K29O constitutes a characteristic of a size exclusion process. Hence, q^{0}_{d} of K29FF and K29O for alkanes like C_7 and C_8 differs in about 9−10 kJ mol^{-1}, whereas the difference is about half of that value (5 kJ mol^{-1}) for C_9 and longer-chain alkanes. Differences between $-\Delta S^{0}_{a}$ of the treated and untreated samples follow a similar trend. This quantitative change indicates that the access to high energy sites is restricted to molecular sizes similar to (or lower than) that of *n*-octane (molecular cross-sectional area, 0.581 nm^2).

The effect of the plasma treatment on the adsorption of polar probes is shown in Figure 6. It can be seen that there exists a noticeable increase of $-\Delta G^{SP}{}_{a}$ values corresponding to the adsorption of acidic (*t*-BuOH) and basic (tetrahydrofuran) probes onto K29O fibers, with respect to those obtained with the K29FF sample. As mentioned before, this can be caused by a slight increment of the nature (strength) or amount of both acidic and basic surface sites. On the other hand, the specific contribution to the overall free energy of adsorption for the apolar (toluene and carbon tetrachloride) and amphoteric (acetone) molecules remains constant after the surface treatment.

Regarding XPS measurements, results of Table 8 reveal a reduction of the atomic C percentage concurrently with an important increase of atomic O in the surface. Nitrogen concentration, on the other hand, remains almost identical (approximately 7%) to that obtained prior to the surface treatment (sample K29FF). High-resolution XPS analysis was performed in K29FF and K29O samples in order to investigate the nature of the oxygen functionalities generated after the plasma oxidation process. Before considering these results furtherly, a remark must be done in the light of data appearing in Table 8. The N/C and O/C ratios obtained for bare aramid surfaces K29FF (0.08 and 0.11 respectively) are rather low with respect to the theoretical prediction for a pristine PPTA fiber (0.14 for both N/C and O/C atomic ratios). These differences cannot be due to slight hydrocarbon contamination, especially in the case of N/C ratio. It seems more likely that some

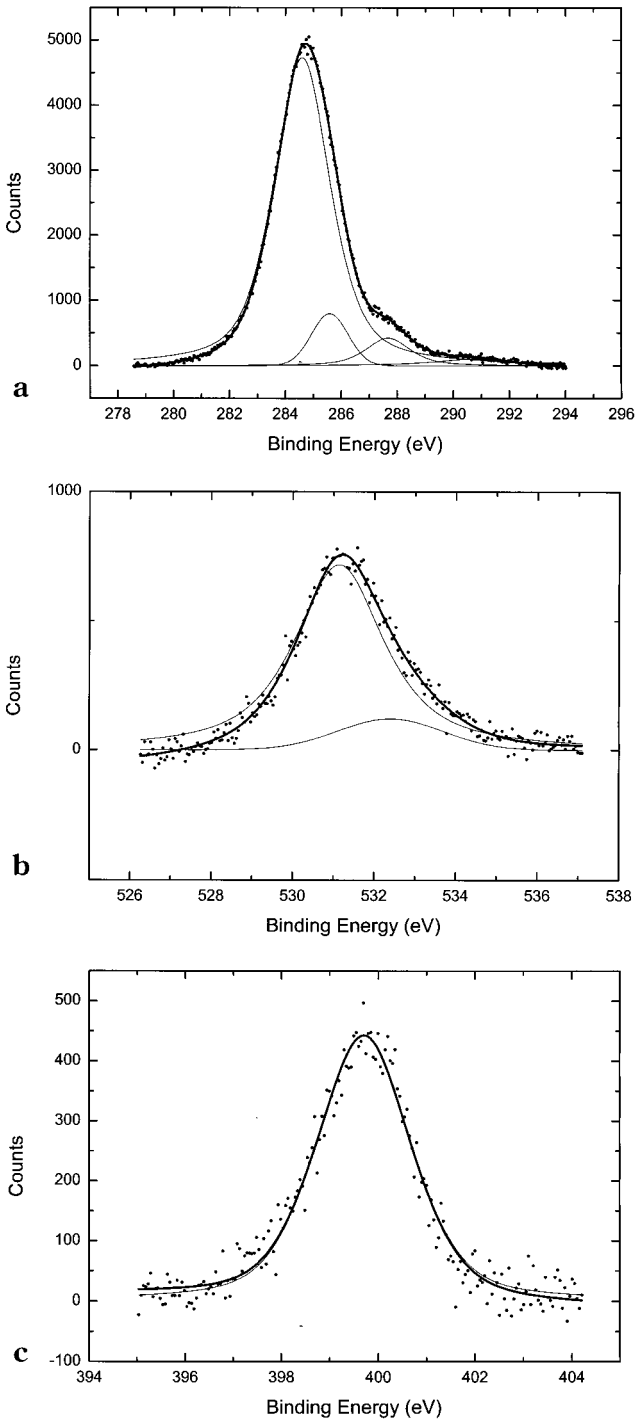

Figure 9. High resolution (a) C 1s, (b) O 1s, and (c) N 1s XPS spectra for untreated K29FF sample

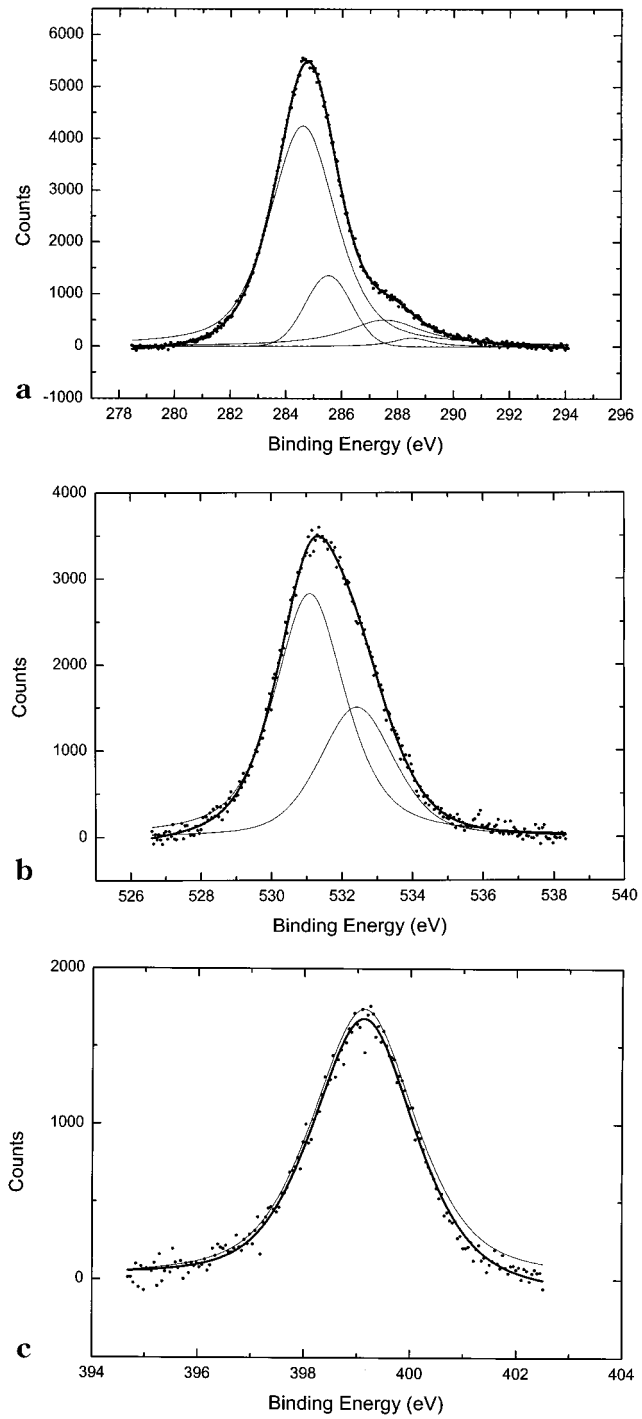

Figure 10. High resolution (a) C 1s, (b) O 1s, and (c) N 1s XPS spectra for plasma-treated K29O sample.

impurities such as those observed in Figure 8a should be contributing to the abnormally high atomic C content detected in the surface of K29FF. Moreover, previous AFM studies on Kevlar fibers similar to sample K29FF detected the contamination spots as being more hydrophobic (i.e., hydrocarbon-like) than the fiber surface.[39] It should be also mentioned that our K29FF atomic composition data (Table 8) agree well with values obtained on Kevlar 29 samples Soxhlet extracted with acetone, as reported by Chappell et al. in their exhaustive XPS analysis of Kevlar fibers with a wide variety of surface treatments.[40]

Correspondingly, Figures 9 and 10 show high-resolution C 1s, O 1s, and N 1s spectra of the untreated K29FF fiber and the plasma oxidized K29O sample. Sample K29FF contains three types of C 1s environments, i.e., C−C, C−N, and N−C═O (Figure 9a). Positions (eV) and relative areas (%) of the three components are collected in Table 9. One additional, much broader peak was obtained at 290.8 eV which is assigned to the $\pi-\pi^*$ shake-up satellite. This peak is excluded from relative area estimations, since the $\pi-\pi^*$ satellite is not attributable to a repeating unit of the PPTA structure.[41] On the other hand, the O 1s envelope of the fresh fiber K29FF is characterized by two peaks (Figure 9b), the major component at approximately 531 eV corresponding to the C═O bond in the amide functionality. A small component shifted to approximately 1 eV of the main peak is assigned to oxygen atoms linked to carbon atoms by single bonds, possibly those forming part of carboxylic moieties. Finally, N 1s core level spectrum can be adequately fitted to a single peak (Figure 9c) assigned to amide groups. Peak positions and relative intensities are detailed in Table 10.

Table 9. Components of K29FF and K29O C 1s Envelopes, with Peak Positions in eV and Relative Areas (in Parentheses) in %

fiber	C−C/C−H	C−N/C−O	N−C═O/C═O	O−C═O
K29FF	284.6 (85)	285.6 (8)	287.7 (7)	
K29O	284.6 (73)	285.5 (14)	287.6 (11)	288.5 (2)

Table 10. O 1s and N 1s Components at K29FF and K29O Samples, with Peak Positions in eV and Relative Areas (in Parentheses) in %

	O 1s		N 1s
fiber	C═O/N−C═O	C−O/C−O−C	N−C═O
K29FF	531.1 (86)	532.4 (14)	399.7
K29O	531.1 (65)	532.4 (35)	399.1

The increment of atomic oxygen observed after plasma treatment is parallel to a decrease of the relative peak area of the C−C component shown in Figure 10a (Table 9). This should be interpreted as a degradation of aromatic rings in the aramid fibers brought about by the highly reactive species present in the plasma environment. Plasma oxidation makes all the other components (C−N/C−O and C═O) to increase after deconvolving the envelope of C 1s. A new peak appears at 288.5 eV (Table 9) assigned to carboxylic groups. The amount of these functionalities is rather low (2%), especially when compared with aramid surfaces oxidized in remote-plasma devices.[42] Analysis of the O 1s high-resolution spectra (Figure 10b) also revealed a substantial increment of the C−O/C−O−C component (Table 10). All this information would indicate that the oxygen introduced after the surface treatment is forming alcoholic or etheric functional groups in the K29O fiber. As expected from results shown in Table 8, the N 1s core level spectra of fibers K29FF and K29O are very similar (Figures 9c and 10c; Table 10).

5. Conclusion

Changes in surface properties of aramid fibers submitted to different treatments have been investigated by means of IGC adsorption studies. On one hand, the use of standard surface finishes has demonstrated to reduce dramatically the surface energy of the fibers, as measured by the dynamic adsorption of *n*-alkanes. Also the surface chemistry of the fibers is highly modified by the presence of surface coatings. In particular, finish-free fibers exhibit a more basic character when com-

pared to the standard (sized) fibers. Processes devoted to remove totally or partially the surface finish such as solvent washing or extraction rendered surfaces with similar structural and chemical properties to those of fresh, finish-free fibers. The effect of plasma treatments on the surface of aramid fibers has been also evaluated. Plasma-treated fibers have shown an enhancement of the enthalpy and entropy of adsorption of linear alkanes. Furthermore, clear size-exclusion behaviors have been observed, probably linked to the formation of pores on the fibers surfaces. AFM measurements confirm radical changes in surface morphology at the nanometer scale after the oxygen plasma treatment, with globular-like structures replacing the microfibrils characteristic of PPTA fibers. As for chemical variations, IGC could only detect an increase of the number and/or strength of the acidic and basic sites present in the fresh fiber. XPS analysis has detected an important increase of surface atomic oxygen as well as the decrease in carbon content at the surface. Deconvolution of high resolution spectra has shown the increase of oxygen moieties (especially of alcohol/ether groups) after plasma oxidation. Overall, IGC has demonstrated to be a very suitable technique to characterize changes in fiber surface properties, with the use of additional techniques, such as scanning probe microscopies or XPS analysis, providing useful complementary information on the changes brought about by surface treatments.

Acknowledgment. Financial support from DGICYT (Project PB98-0492) and FICYT (Project PB-EXP01-06) is gratefully acknowledged. XPS measurements were carried out at Loughborough University under the supervision of Drs. A. Cuesta and R. H. Bradley. M.A.M-M. thanks the FICYT (Spain) for a personal grant.

References and Notes

(1) Yang, H. H. *Aromatic High-Strength Fibers*; Wiley: New York, 1989.
(2) Yang, H. H. In *Fibre Reinforcement for Composite Materials*; Bunsell, A. R., Ed.; Elsevier: Amsterdam, 1988; p 249.
(3) de Lange, P. J.; Mahy, J. W. G. *Fresenius J. Anal. Chem.* **1995**, *353*, 487−493.
(4) Van Asten, A.; van Veenendaal, N.; Koster, S. *J. Chromatogr. A* **2000**, *888*, 175−196.
(5) Chan, C.-M.; Ko, T.-M.; Hiraoka, H. *Surf. Sci. Rep.* **1996**, *24*, 1−54.
(6) Bosse, F.; Schreiber, H. P.; Eisenberg, A. *Macromolecules* **1993**, *26*, 6447−6454.
(7) Mukhopadhyay, P.; Schreiber, H. P. *Macromolecules* **1993**, *26*, 6391−6396.
(8) Glass, A. S.; Larsen, J. W. *Macromolecules* **1993**, *26*, 6354−6358.
(9) Wang, J. Y.; Charlet, G. *Macromolecules* **1993**, *26*, 2413−2419.
(10) Lloyd, D. R., Ward, T. C., Schreiber, H. P., Pizaña, C. C., Eds.; *Inverse Gas Chromatography. Characterization of Polymers and Other Materials*; ACS Symposium Series 391; American Chemical Society: Washington, DC, 1989.
(11) Conder, J. R.; Young, C. L. *Physicochemical Measurements by Gas Chromatography*; Wiley: Chichester, England, 1979.
(12) Sherwood, P. M. A. In *Practical Surface Analysis*, 2nd ed.; Briggs, D., Seah, M. P., Eds.; Wiley: Chichester, England, 1990; Vol 1, p 555.
(13) De Boer, J. H. *The Dynamic Character of Adsorption*; Clarendon Press: Oxford, England, 1953.
(14) Dorris, G. M.; Gray, D. G. *J. Colloid Interface Sci.* **1980**, *77*, 353−362.
(15) Gutmann, V. *The Donor-Accpetor Approach to Molecular Interactions*; Plenum Press: New York, 1979.
(16) Riddle, F. L.; Fowkes, F. M. *J. Am. Chem. Soc.* **1990**, *112*, 3259−3264.
(17) Panzer, U.; Schreiber, H. P. *Macromolecules* **1992**, *25*, 3633−3637.
(18) Donnet, J. B.; Park, S. J.; Balard, H. *Chromatographia* **1991**, *31*, 434−440.
(19) Chappell, P. J. C.; Williams, D. R. *J. Adhes. Sci. Technol* **1990**, *4*, 7−16.
(20) Clark, A. *The Theory of Adsorption and Catalysis*; Academic Press: New York, 1970.
(21) Rebouillat, S.; Donnet, J. B.; Guo, H.; Wang, T. K. *J. Appl. Polym. Sci.* **1998**, *67*, 487−500.
(22) Chappell, P. J. C.; Williams, D. R. *J. Colloid Interface Sci.* **1989**, *128*, 450−457.
(23) Rebouillat, S.; Escoubes, M.; Gauthier, R.; Vigier, A. *J. Appl. Polym. Sci.* **1995**, *58*, 1305−1315.
(24) Hsieh, Y.-L.; Wu, M.; Andres, D. *J. Colloid Interface Sci.* **1991**, *144*, 127−144.
(25) Vukov, A. J.; Gray, D. G. *Langmuir* **1988**, *4*, 743−748.
(26) Gozdz, A. S.; Weigmann, H.-D. *J. Appl. Polym. Sci.* **1984**, *29*, 3965−3979.
(27) Paredes, J. I.; Martínez-Alonso, A.; Tascón, J. M. D. *Langmuir* **2001**, *17*, 474−480.
(28) Riekel, C.; Dieing, T.; Engström, P.; Vincze, L.; Martin, C.; Mahendrasingam, A. *Macromolecules* **1999**, *32*, 7859−7865.
(29) Snétivy, D.; Vancso, G. J.; Rutledge, G. C. *Macromolecules* **1992**, *25*, 7037−7042.
(30) Rebouillat, S.; Peng, J. C. M.; Donnet, J.-B. *Polymer* **1999**, *67*, 7341−7350.
(31) Li, S. F. Y.; McGhie, A. J.; Tang, S. L. *Polymer* **1993**, *34*, 4573−4575.
(32) Nie, H.-Y.; Walzak, M. J.; McIntyre, N. S. *Appl. Surf. Sci.* **1999**, *144*−*145*, 627−632.
(33) O'Kell, S.; Henshaw, T.; Farrow, G.; Aindow, M.; Jones, C. *Surf. Interface Anal.* **1995**, *23*, 319−327.
(34) Montes-Morán, M. A.; Paredes, J. I.; Martínez-Alonso, A.; Tascón, J. M. D. *J. Colloid Interface Sci.* **2002**, *247*, 290−302.
(35) Paredes, J. I.; Martínez-Alonso, A.; Tascón, J. M. D. *Carbon* **2000**, *38*, 1183−1197.
(36) Brendlé, E.; Papirer, E. *J. Colloid Interface Sci.* **1997**, *194*, 207−216.
(37) Everett, D. M.; Powl, J. C. *J. Chem. Soc., Faraday Trans. 1* **1976**, *72*, 619−636.
(38) Lopez-Garzón, F. J.; Pyda, M.; Domingo-García, M. *Langmuir* **1993**, *9*, 531−536.
(39) Paredes, J. I.; Martínez-Alonso, A.; Tascón, J. M. D. *J. Microscopy* **2000**, *200*, 109−113.
(40) Chappell, P. J. C.; Williams, D. R.; George, G. A. *J. Colloid Interface Sci.* **1990**, *134*, 385−396.
(41) Inagaki, N.; Tasaka, S.; Kawai, H. *J. Polym. Sci. A, Polym. Chem.* **1995**, *33*, 2001−2011.
(42) Inagaki, N.; Tasaka, S.; Kawai, H.; Yamada, Y. *J. Appl. Polym. Sci.* **1997**, *64*, 831−840.

MA020069M